

Detecting the foreign matter defect in lithium-ion batteries based on battery pilot manufacturing line data analyses



Yue Pan^a, Xiangdong Kong^{a,*}, Yuebo Yuan^a, Yukun Sun^a, Xuebing Han^a, Hongxin Yang^b, Jianbiao Zhang^b, Xiaoan Liu^b, Panlong Gao^b, Yihui Li^{b,c}, Languang Lu^a, Minggao Ouyang^{a,**}

^a State Key Laboratory of Automotive Safety and Energy, Tsinghua University, Beijing, 100084, China

^b SVOLT Energy Technology Co., Ltd, Changzhou, 213200, China

^c Dr. Octopus Intelligent Technology (Shanghai) Co., Ltd, Shanghai, 201800, China

ARTICLE INFO

Keywords:

Lithium-ion battery
Battery safety
Foreign matter defect
Defect detection
Data-driven method

ABSTRACT

Foreign matter defect introduced during lithium-ion battery manufacturing process is one of the main reasons for battery thermal runaway. Therefore, reliable detection of the foreign matter defect is needed for safe and long-term operation of lithium-ion batteries. It is favored to detect the defective battery during the battery manufacturing process before the battery is put into use. In this study, the defects are implanted into batteries on a real battery pilot manufacturing line. Data of defective batteries and thousands of normal batteries are collected for data analyses and algorithm development. Feature selection is conducted with feature importance analysis using the random forest method and out-of-bag error calculation. Local outlier factor method is used for defect detection with the selected features as input. The proposed defect detection algorithm achieves high detection rate and low false alarm rate which has the potential to be deployed on the manufacturing execution system to further enhance screening ability of defective batteries and improve battery safety.

1. Introduction

Due to the environmental pollution, global warming and energy crisis, countries around the world are seeking to replace fuel vehicles with new energy vehicles to alleviate the resource crisis and reduce greenhouse gas emissions [1,2]. Lithium-ion battery, with the advantage of high energy density, high power density and long cycle life, is widely used as the power source for electric vehicles [3,4]. In the field of energy storage, lithium-ion battery is also anticipated to be the dominating battery energy storage solution, owing to its advances in operational characteristics and price reductions [5,6]. In the past three decades, lithium-ion batteries have made great progress in terms of cost, energy density, cycle life and safety [7]. However, with the mass production and widespread use of lithium-ion batteries, many safety accidents caused by the thermal runaway of lithium-ion batteries occurred worldwide, resulting in severe losses and hindering the further spread of battery applications [8,9].

From the perspective of battery usage, thermal runaway is believed to be caused by battery abuse conditions which can be categorized into

mechanical abuse [10,11], electrical abuse [12] and thermal abuse [13]. In order to avoid battery abuse and mitigate the damage caused by battery abuse, numerous studies have been conducted in the areas of battery forward development [14,15], thermal management [16,17], state estimation [18,19], battery diagnosis [20,21], etc. From the perspective of battery quality itself, defects introduced in the battery manufacturing process can severely affect battery quality [22], causing abnormal capacity degradation and safety problems [23]. As is disclosed in some vehicle recall notice announced by China State Administration for Market Regulation, defects inside the battery is one of the causes of thermal runaway accidents [24,25]. Therefore, it is highly essential to study the impact of battery defects on battery safety.

Different types of defects can be introduced into batteries during the battery manufacturing process, such as pinholes, metal particles, non-uniform coating, burrs or rips on the tab, deflected electrode, etc. [22, 26]. Among all kinds of defects, the foreign matter defect (FMD) is a severe problem which can be introduced in almost every process of battery manufacturing: Foreign matter such as Fe, Al, Mg, Cu and Si particles may be present in battery raw material made from recycled batteries [27–29]; Non-magnetic particles can be easily introduced into

* Corresponding author.

** Corresponding author.

E-mail addresses: yuepan_thu@foxmail.com (Y. Pan), ouymg@tsinghua.edu.cn (M. Ouyang).

Nomenclature	
<i>Abbreviation, description</i>	
BS	Bootstrap
DT	Decision Trees
FI	Feature Importance
FMD	Foreign Matter Defect
FN	False Negative
FP	False Positive
HiPot	High Potential
IR	Internal Resistance
ISC	Internal Short Circuit
LOF	Local Outlier Factor
NG	Not Good
RF	Random Forest
TN	True Negative
TP	
304S	
<i>Variable or parameter, description</i>	
$d(p, q)$	the Euclidean distance between object p and q
<i>Subscript, description</i>	
i	Denote the i th input and output
j	Denote the j th DT, BS and prediction
TP	True Positive
304	Stainless Steel
<i>Superscript, description</i>	
m	Denote the input, OOB error and feature importance with feature m randomly shuffled

the slurry during the slurry mixing, transporting and storage which are difficult to be removed [30]; Welding slag, a large-size metallic particle, can be introduced during the welding process [31]. The existing studies have demonstrated that FMD may cause fast battery degradation and internal short circuit (ISC): Mohanty et al. compared the electrochemical performance and degradation mechanism of different types of defects with coin cells and they found that the metal particle defect caused poor rate capability and fast capacity degradation [26]. Liu et al. demonstrated that iron particles can induce the internal short circuit when cycling the cells by implanting the iron particles into 1Ah pouch cells [32]. The researchers from General Motors also implanted iron particles with different sizes into 1.4Ah pouch cells and concluded that metal particles located on the positive electrode can cause ISC [33]. Recent study from our group also proved that FMD defects can be the intrinsic cause of thermal runaway: the sudden spontaneous combustion can be caused by FMD defect without abuse [34,35]. Therefore, the detection of FMD is of significance to improve battery safety.

Numerous battery defect detection methods have been developed and applied in battery manufacturing process. In the electrode preparation process, X-ray radiography [36], acoustic guided waves [37], thermography [38] and computer vision methods [39,40] are used for electrode coating defects detection. In the battery assembly process, computed tomography [41] and X-ray [42] are used for electrode protrusions and wrinkles detection. In the battery finishing process, scanning acoustic microscopy [43], thermography [44] and computer vision [45] methods are used for blister defect detection. In case of FMD detection, High Potential (HiPot) test, a test method used in the electrical safety assessment, is widely used in the battery manufacturing line [46]. HiPot test realizes the detection of FMD by examining the insulation performance of the battery. Hoffmann et al. conducted HiPot test to single-layer cell and demonstrated that one single particle with the diameter of $\sim 80 \mu\text{m}$ can be detected [47]. However, the HiPot test does not yield satisfactory results in the pilot manufacturing line used in this study. Therefore, new FMD detection methods with high reliability

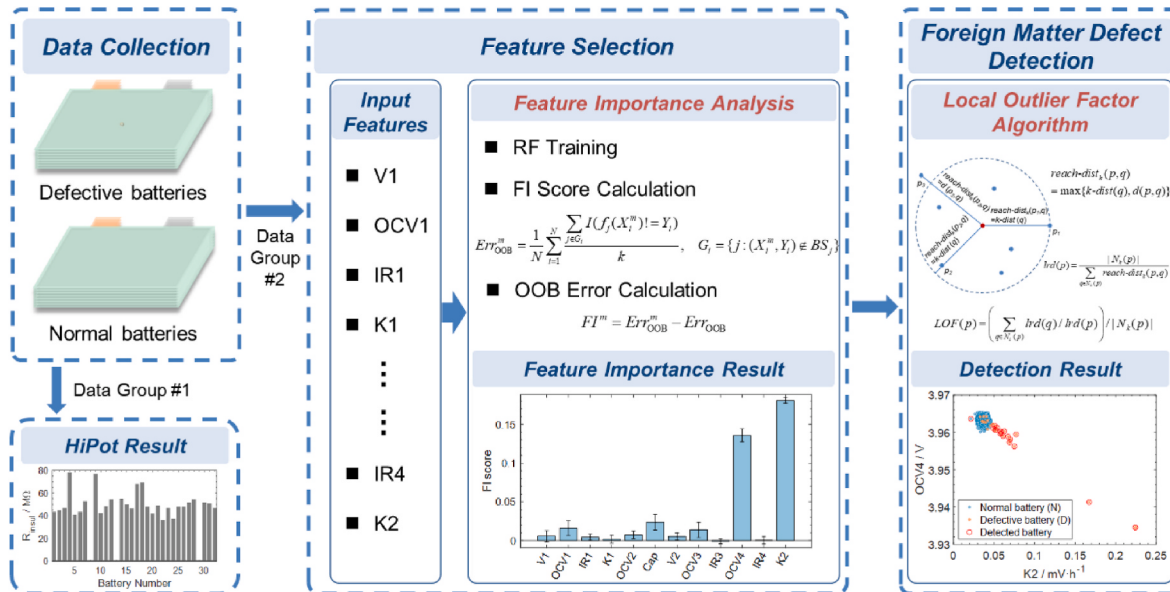


Fig. 1. The flowchart of the FMD detection method based on battery pilot manufacturing line data analyses.

(high detection rate and low false alarm rate) are needed.

In this paper, a detection method of FMD based on battery pilot manufacturing line data analyses is introduced, as is shown in Fig. 1. Compared with the existing studies conducted at laboratory level with handmade coin cells or small pouch cells, we implanted the FMD into commercial large-capacity batteries during the battery assembly process in the battery pilot manufacturing line, which kept the experimental conditions much closer to reality. The details of the experiment setup are introduced in Section 2. In Section 3, the data analyses method based on random forest (RF) classification and out-of-bag error calculation are introduced. Then, the defect detection method is developed based on the Local Outlier Factor (LOF) algorithm. Section 4 presents the detection results of the proposed method. Necessary discussions on false negative analysis and computational efficiency are conducted. Finally, conclusions of this study and outlook of the next-step work are provided in Section 5.

2. Experiments and data collection

2.1. Defect batter production

The battery used in this study is a prismatic lithium-ion battery with a nominal capacity of 114Ah. The detailed information of the battery is listed in Table 1.

The defect implanting process is illustrated in Fig. 2. Firstly, in order to keep the experiment condition as close as possible to the battery manufacturing conditions, jelly rolls after stacking were collected from the pilot manufacturing line. The jelly roll is a semi-finished cell of the battery assembly process which is covered with a green insulation film. Next, the jelly roll was carefully opened and one foreign matter particle was implanted into it. Then, the jelly roll was resealed and re-entered the pilot manufacturing line. The foreign matter particle was put in the center of the large surface of cathode, as is shown in Fig. 2. Totally thirty-two defect batteries with different particle materials and sizes were produced. The materials of the foreign matter particles used in this study are copper (Cu) and 304 stainless steel (304S, an austenitic stainless steel, chemical formula Cr₁₈Ni₈). The diameters of the particles are from 150 μm to 450 μm. The detailed information of the defect batteries can be found in Table 2.

2.2. Data collection

The FMD was implanted to the jelly roll in the battery assembly process. The defect jelly roll re-entered the pilot manufacturing line and went through the subsequent manufacturing process and data were collected. It is worth noting that all the defect batteries followed the original manufacturing process without adding additional tests or inspections. During the manufacturing process, battery characteristic parameters such as the battery voltage and internal resistance are collected by the manufacturing execution system. Since the FMD was implanted in the battery assembly process, only the battery characteristic parameters

after defect implanting are analyzed in this study. Totally 15 battery characteristic parameters were collected for further analyzation, as is listed in Table 3.

The 15 parameters in Table 3 are divided into 2 groups. Group #1 are the parameters of HiPot test. HiPot test is used in the polit manufacturing line to detect the FMD. The insulation resistance is measured by the HiPot test with a voltage of 250 V. One HiPot test is conducted for the jelly roll after the hot-pressing process measuring the insulation resistance between negative tab and positive tab. Two HiPot tests are conducted for the battery which measure the insulation resistance between negative tab and positive tab, negative tab and aluminum housing respectively. If the insulation resistance is lower than the standard of the manufacturing line, the HiPot test give a Not Good (NG) signal, which means the jelly roll or the battery fails to pass the HiPot test. The jelly roll or battery that fails to pass the HiPot will be intercepted by the manufacturing execution system and no subsequent manufacturing processes will be carried out, which means that its subsequent parameters will be missing. The parameters of Group #1 are used to evaluate the FMD detection capability of the HiPot test.

Group #2 are the parameters of battery finishing process. Only the batteries that passed the HiPot tests have Group #2 parameters. Group #2 parameters include terminal voltage, open circuit voltage (OCV) and internal resistance measured at different steps of the battery finishing process, containing precharging, high temperature aging, formation and room temperature aging. Two K-values are also measured, which are defined as the ratio of voltage change over time during battery resting. The K-values are indicators of battery self-discharge, which are widely used in battery manufacturing process [48]. The parameters of Group #2 are used to develop the FMD detection algorithm that will be introduced in the next section.

Besides the 32 defect batteries listed in Table 2, data of thousands of normal batteries from the same batch with the defect batteries are also collected. Totally 3965 batteries (32 FMD batteries and 3933 normal batteries) are collected for further investigation in this study.

3. Methodology

Since the FMD occurs with relatively low possibility in battery manufacturing process, the detection of FMD is an anomaly detection problem. As is listed in Table 3, 12 battery parameters (features) of Group #2 are collected and used for anomaly detection. (The word “parameters” and “features” have different meanings in algorithms. “Features” usually refer to the input of algorithms. Therefore, “feature” which means “battery parameter” is used in the following parts to avoid ambiguities and misunderstandings.) However, not all the features are important for the FMD detection. Feature importance analysis is conducted first to select the appropriate features. Then, the FMD detection algorithm is developed using the selected features.

3.1. Feature selection method

The random forest method is a commonly used tool for classification or regression purposes. A key advantage of the RF method over alternative machine learning algorithms is the measure of feature importance, which can be used to identify relevant features or perform feature selection [49].

In the RF algorithm, several individual decision trees (DT) are combined to make final classification or regression. In this study, the RF is used as a classification algorithm with a dataset $\{(X_1, Y_1), (X_2, Y_2), \dots, (X_N, Y_N)\}$ containing N observations (batteries), where X_i denotes the input vector with M features and Y_i denotes the output categories (In this study, $M = 12$. $Y_i = 1$ for defect batteries and $Y_i = 0$ for normal batteries). For classification, the result of the RF is the majority vote of the results of all DTs in the forest. Each DT is fitted on a random bootstrap (BS) dataset. Observations which are not used to construct a DT are termed out-of-bag (OOB) observations for that DT. A randomly chosen

Table 1

Detailed information of the batteries under investigation.

Detailed information	Battery
Nominal capacity	114 Ah
Cathode material	NCM
Anode material	Graphite
Battery type	Prismatic
Charging cutoff voltage	4.2 V
Discharging cutoff voltage	2.8 V
Working temperature	-30–55 °C
Energy density	227 Wh/kg
Length	147.5 ± 0.6 mm
Height	105.8 ± 0.4 mm
Thickness	52.3 ± 0.3 mm

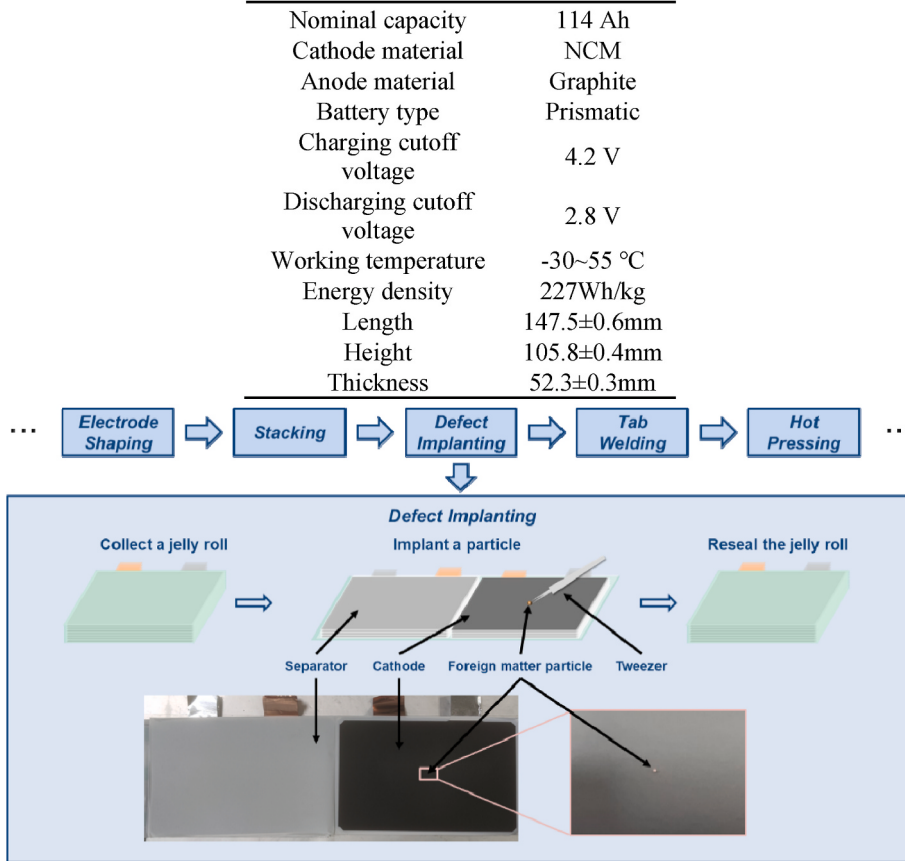


Fig. 2. The illustration of the defect implanting process.

Table 2

Detailed information of the defect batteries.

Particle material	Particle diameter	Battery number	Quantity
Cu	150 μm	No. 1-2	2
Cu	250 μm	No. 3-4	2
Cu	350 μm	No. 5-6	2
Cu	450 μm	No. 7-16	10
304S	150 μm	No. 17-18	2
304S	250 μm	No. 19-20	2
304S	350 μm	No. 21-22	2
304S	450 μm	No. 23-32	10

subset of features is assessed as candidates for each split in each DT. In the version of RF proposed by Breiman, the selected split is the split with the largest decrease in Gini impurity [50]. Each DT can be trained with different BS datasets and make different splits, which leads to an increased diversity of DTs and increases the noise immunity of RF.

$$\begin{cases} I(x) = \begin{cases} 1, & x = \text{True} \\ 0, & x = \text{False} \end{cases} \\ Err_{OOB} = \frac{1}{N} \sum_{i=1}^N \sum_{j \in G_i} I(f_j(X_i) \neq Y_i) \end{cases}, G_i = \{j : (X_i, Y_i) \notin BS_j\} \quad (1)$$

After the training of RF, the OOB observations of each DT can be used to evaluated the performance of the RF. The OOB error (Err_{OOB}) is defined in Eq. (1), where BS_j is the bootstrap used to train the j th DT, (X_i, Y_i) denotes the i th input and output, G_i denotes a set of BS_j satisfying $(X_i, Y_i) \notin BS_j$, $f_j(X_i)$ denotes the prediction of the j th DT taking X_i as input, function $I(x)$ is a one-zero judgment function. According to the definition of Err_{OOB} , A small Err_{OOB} value indicates good performance of the

Table 3

Battery characteristic parameters used in this study.

Group	Name	Description
Group #1: Parameters of HiPot tests	HiPot1	HiPot test result for jelly roll after hot-pressing
	HiPot2	HiPot test result for battery negative and positive tab
	HiPot3	HiPot test result for battery negative tab and housing
Group #2: Parameters of battery finishing process	V1	Terminal voltage after precharging
	OCV1	OCV after precharging
	IR1	Internal resistance after precharging
	K1	K-value after high temperature aging
	OCV2	OCV before formation
	Cap	Battery capacity
	V2	Terminal voltage after formation
	OCV3	OCV after formation
	IR3	Internal resistance after formation
	OCV4	OCV after room temperature aging
	IR4	Internal resistance after room temperature aging
	K2	K-value after room temperature aging

RF. Then the feature importance (FI) is defined to be the increase of Err_{OOB} when a single feature is randomly shuffled [51]. This shuffling procedure breaks the relationship between the feature and the target, thus the increase in Err_{OOB} is indicative of how much the RF model depends on the shuffled feature. If feature m is important to the output, a large Err_{OOB} is expected after randomly shuffling feature m . Therefore, FI of feature m can be defined in Eq. (2), where feature m is randomly shuffled among all the inputs to get a new dataset $\{(X_1^m, Y_1), (X_2^m, Y_2), \dots, (X_N^m, Y_N)\}$, Err_{OOB}^m denotes the OOB error of feature m with the new dataset and FI^m denotes the FI of feature m .

$$\begin{cases} Err_{\text{OOB}}^m = \frac{1}{N} \sum_{i=1}^N \frac{\sum_{j \in G_i} I(f_j(X_i^m) \neq Y_i)}{k}, G_i = \{j : (X_i^m, Y_i) \notin BS_j\} \\ FI^m = Err_{\text{OOB}}^m - Err_{\text{OOB}} \end{cases} \quad (2)$$

The overall procedure of the feature importance analysis is summarized in Table 4. The features that have large FI score are the selected features for FMD detection.

3.2. Foreign matter defect detection

The Local Outlier Factor (LOF) algorithm, an unsupervised anomaly detection method firstly proposed by Breunig et al. is a well-known algorithm for detecting local outliers [52]. Recent studies have also applied the LOF algorithm to fault diagnosis of lithium-ion battery used in electric vehicles [53]. In this study, the LOF algorithm is used for FMD detection using the selected features.

The LOF algorithm is a density-based method which measures the local deviation of the density of a given sample with respect to its neighbors. The lower the density of the point, the more likely it is to be identified as the outlier. The key definitions of the LOF algorithm are briefly introduced as follows:

Definition 1. $d(p, q)$: $d(p, q)$ is the Euclidean distance between object p and q . In this study, each battery is taking as an object and the selected features (after normalization) are the coordinates of the object.

Definition 2. k -distance: For positive integer k , sort the distances from object p to other objects in ascending order. The distance from p to the k th object is defined as k -distance and denoted as $k\text{-dist}(p)$.

Definition 3. k nearest neighbors: A set of the objects whose distance to object p are no more than $k\text{-dist}(p)$ is defined as k nearest neighbors of object p , denoted as $N_k(p)$. $|N_k(p)|$ denotes the size of set $N_k(p)$.

Definition 4. reachability distance: The reachability distance of object p with respect to object q , denoted as $\text{reach-dist}_k(p, q)$, is defined in Eq. (3).

$$\text{reach-dist}_k(p, q) = \max\{k\text{-dist}(q), d(p, q)\} \quad (3)$$

Definition 5. local reachability density: The local reachability density of object p , denoted as $\text{lrd}(p)$, is defined in Eq. (4).

$$\text{lrd}(p) = 1 / \left(\frac{\sum_{q \in N_k(p)} \text{reach-dist}_k(p, q)}{|N_k(p)|} \right) \quad (4)$$

Definition 6. local outlier factor: LOF of object p is defined in Eq. (5).

$$\text{LOF}(p) = \frac{\sum_{q \in N_k(p)} \text{lrd}(q)}{|\text{lrd}(p)|} \quad (5)$$

Table 4
The procedure of feature importance analysis.

Procedure	Description
1. RF Training	Train the RF model using the original dataset $\{(X_1, Y_1), (X_2, Y_2), \dots, (X_N, Y_N)\}$.
2. OOB error Calculation	Calculate OOB error with original dataset to get Err_{OOB} .
3. FI score Calculation	For $m = 1$ to M (M is the number of features): a. Randomly shuffle feature m to get a new dataset $\{(X_1^m, Y_1), (X_2^m, Y_2), \dots, (X_N^m, Y_N)\}$. b. Calculate OOB error with the new dataset to get Err_{OOB}^m . c. Calculate the feature importance of feature m

In this study, the LOF value of each battery is calculated with the selected features as input. The batteries with large LOF value can be detected with a threshold value. The exact hyperparameter settings and the detection results will be introduced in the next section.

4. Results and discussions

4.1. HiPot results for jelly rolls and batteries

The HiPot results of the FMD jelly rolls and batteries are shown in Fig. 3. The insulation resistance R_{insul} is measured by the HiPot test with a voltage of 250 V. The standard of R_{insul} is $1\text{M}\Omega$ for the pilot manufacturing line, which means that the HiPot test will give NG signals for jelly roll and battery whose R_{insul} is smaller than $1\text{M}\Omega$. As is shown in Fig. 3(a), three jelly rolls (Number 8, 13 and 29 in Table 2) do not pass the HiPot test. These three jelly rolls are intercepted by the manufacturing execution system and their subsequent test results are missing (HiPot2, HiPot3 and all the parameters of Group#2 in Table 3 are missing). Except for these three jelly rolls, the other jelly rolls passed the HiPot tests with the insulation resistance larger than $15\text{M}\Omega$. The detailed HiPot test results can be found in Table S1 in the supplementary material.

All the NG signals come from $\text{HiPot1} < 1\text{M}\Omega$, which is measured on the jelly roll after hot-pressing. Noting that the implanted particle size is far larger than the thickness of separator, cathode and anode, it is assumed that separators and electrodes may be pierced in some jelly rolls at the hot-pressing process which reduces the insulation resistance. If the implanted particle does not pierce the separators and electrodes during hot-pressing, the jellyroll can pass the HiPot test. After welding and enclosing, the corresponding battery can also pass the HiPot tests. Only three FMD batteries (Number 8, 13 and 29 in Table 2) with an FMD particle size of $450\text{ }\mu\text{m}$ can be detected by the HiPot tests. The detection rate of HiPot tests is 9.4% (3/32). Therefore, HiPot tests used in the pilot manufacturing line are not reliable enough for FMD detection. Further

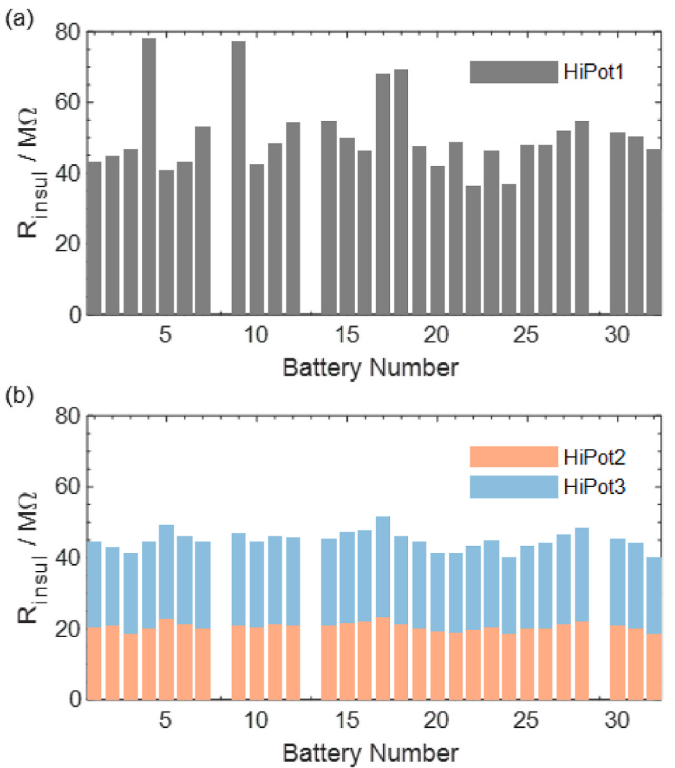


Fig. 3. (a)The HiPot results of the FMD jelly rolls (b) The HiPot results of the FMD batteries.

analyses and other detection methods based on the parameters of battery finishing process are highly required.

4.2. Results of feature selection

Firstly, a binary classification RF model is trained using the original dataset containing 29 FMD batteries and 3933 normal batteries. The normal batteries and the FMD batteries are from the same batch. 12 features in Group #2 listed in Table 2 are taken as the inputs of RF model, while the label ($Y = 1$ for defective battery and $Y = 0$ for normal battery) is used as the output. Since the number of FMD batteries is far less than the number of the normal batteries, the weight of the two classes are adjusted to be inversely proportional to the class frequencies of the input data. The number of DT is set to 30 which is large enough to ensure OOB error calculation.

The FI score of all the features are calculated with each feature shuffled 20 times. As is shown in Fig. 4, the height of each bar is the mean value of all the shuffling, while the error bar shows the standard deviation. The FI score of K1, IR3 and IR4 are close to zero, indicating that these features make no contributions to FMD detection. V1, OCV1, IR1, OCV2, Cap, V2 and OCV3 have small FI score, indicating that these features are of little importance for FMD detection. K2 and OCV4 have the highest FI score which means they are the two most important features that can be used for FMD detection.

4.3. Results of the FMD detection

The selected features K2 and OCV4 are taken as the input of the LOF algorithm. The number of the neighbors k is set to be 200. The threshold value T_{LOF} is set to be 2.85, the battery with the LOF value larger than T_{LOF} is considered as anomaly. The values of these two hyperparameters will be changed and discussed later.

The FMD detection result is shown in Fig. 5. The LOF value is calculated and plotted in descending order in Fig. 5(a), where the FMD batteries are colored in orange and the normal batteries are colored in blue. Apparently, 18 FMD batteries have large LOF values and therefore can be detected (18 FMD batteries out of the top 20 batteries). The exact detection results are marked in red circles in the OCV4–K2 scatter plot, as is shown in Fig. 5(b). The detected FMD batteries have larger K2 value and smaller OCV4 value than the normal batteries, while the K2 and OCV4 value of the undetected FMD batteries are similar with those of normal batteries. Therefore, not all the FMD batteries can be detected by the algorithm.

Recall, Precision, Accuracy and F1-score are four indicators to evaluate the effectiveness of anomaly detection algorithm, as is defined in Eq. (6). Recall is an indicator of detection rate while Precision is an

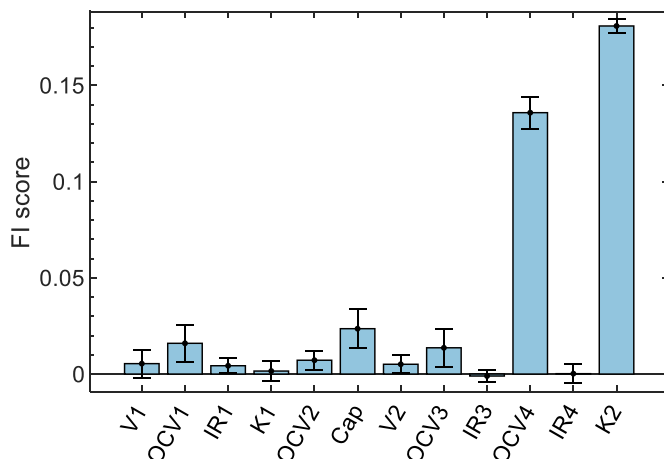


Fig. 4. Feature importance scores for all the 12 features.

indicator of false alarm rate. F1-score is the harmonic mean of Recall and Precision, hence it can be considered as a comprehensive indicator of detection rate and false alarm rate. The confusion matrix in Fig. 4(b) clearly indicates that the true positive (TP) value equals to 18, true negative (TN) value equals to 3932, false positive (FP) value equals to 1 and false negative (FN) equals to 11. The Recall, Precision, F1-score and Accuracy are calculated and shown in the following: Recall = 62.07%, Precision = 94.74%, F1-score = 75.00% and Accuracy = 99.70%.

$$\left\{ \begin{array}{l} \text{Recall} = \frac{\text{TP}}{\text{TP} + \text{FN}} \\ \text{Precision} = \frac{\text{TP}}{\text{TP} + \text{FP}} \\ \text{F1-score} = \frac{2 \times \text{Recall} \times \text{Precision}}{\text{Recall} + \text{Precision}} \\ \text{Accuracy} = \frac{\text{TP} + \text{TN}}{\text{TP} + \text{FP} + \text{TN} + \text{FN}} \end{array} \right. \quad (6)$$

The detailed detection results of the LOF algorithm are listed in Table 5. From the aspect of defect material, slightly more batteries with Cu particles than those with 304S particles are detected. From the aspect of defect particle size, the particle size from 150 μm to 450 μm can be detected with only 150 μm 304S as an exception, which may be due to the small number of FMD batteries in each category with the particle diameter less than 450 μm . The comparison among different FMD categories is not the focus of this study. In the following discussions, the difference among FMD materials and particle diameters will not be distinguished and compared.

4.4. Discussions on hyperparameter tuning

The hyperparameters k and T_{LOF} have significant influence on the detection results. With specific k and T_{LOF} values, the Recall and Precision can achieve 100% respectively. However, there is usually a trade-off relationship between Recall and Precision. The values of the hyperparameters are changed and the corresponding Recall, Precision, F1-score and Accuracy are shown in Fig. 6.

The hyperparameter k influence the calculation of LOF. With a constant T_{LOF} value, the four indicators changed significantly with k when the k value is small (smaller than around 50). However, when the k value becomes larger, the four indicators change slightly with k . The hyperparameter T_{LOF} directly determine the classification process based on the calculated LOF scores. Therefore, T_{LOF} has significant influence on the four indicators. When the k value is constant, the Precision and Accuracy increase while the Recall decreases as T_{LOF} increases. The Accuracy can easily achieve >95% with a wide range of T_{LOF} and k since the number of normal batteries is far larger than the number of FMD batteries. However, the maximum of F1-score is only 75% due to the trade-off relationship between Recall and Precision. The F1-score can be a comprehensive indicator of detection rate (Recall) and false alarm rate (1-Precision). Therefore, the F1-score is maximized and the corresponding hyperparameters and other indicators are listed in Table 6.

As is listed in Table 6, the Recall, Precision and Accuracy have the same values under different hyperparameter combinations when F1-score is maximized. The Recall, Precision and Accuracy values in Table 6 are the final results of the detection method introduced in this study. The Recall value is 62.07% (18/29), which is three times higher than that of the HiPot test 9.38% (3/32). However, compared with the high Precision and Accuracy, the Recall is relatively low. Therefore, the false negative analysis is further discussed.

4.5. Discussions on false negative analysis

The detected FMD batteries are marked as true positive (TP) results while the undetected FMD batteries are marked as false negative (FN) results in the confusion matrix. The unsupervised anomaly detection

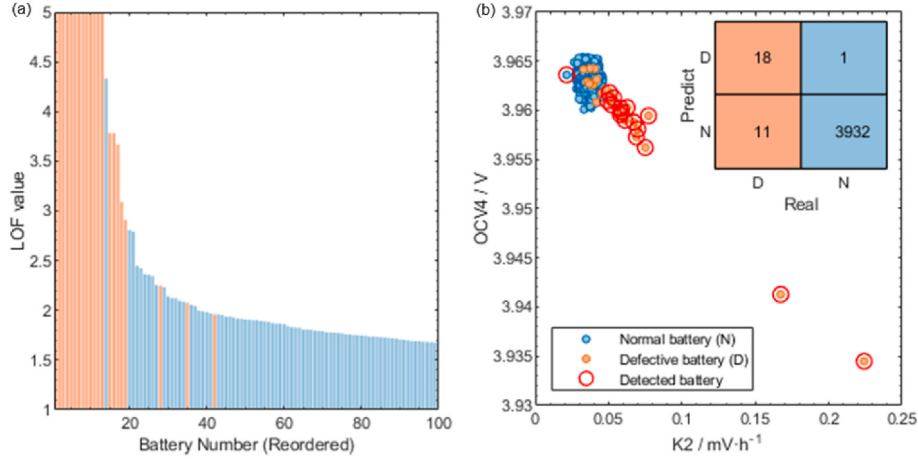


Fig. 5. The FMD detection result. (a) The LOF value of top 100 batteries. (b) The OCV4–K2 scatter plot with confusion matrix.

Table 5
Detailed results of the detected batteries.

FMD information	Number	Quantity
Cu,150 μm	No. 1	1
Cu,250 μm	No. 3,4	2
Cu,350 μm	No. 5	1
Cu,450 μm	No. 7,10,11,12,14,15	6
304S,150 μm	/	0
304S,250 μm	No. 19	1
304S,350 μm	No. 21	1
304S,450 μm	No. 24,25,27,30,31,32	6

methods assume that the feature distributions of anomalous and normal samples are different. FN results occurs when they have similar distribution with normal samples.

According to the definition of Recall in Eq. (6), large FN value causes small Recall. As is shown in Fig. 5(b), some FMD batteries colored in orange is mixed with the normal batteries. These FMD batteries are the FN results of the detection algorithm. To make it clearer, Fig. 7 shows the distribution of K2 and OCV4 of normal batteries and FMD batteries. The probability is calculated assuming a normal distribution of K2 and OCV4 of normal batteries and is plotted in blue. Bar plot is used for FMD

batteries colored in orange for TP and red for FN since the number of FMD batteries is not enough to calculate a distribution. All the FN bars in Fig. 7(a) and (b) are overlapped with the distribution of normal batteries, which explains why they are not detected.

Except for K2 and OCV4, there are 10 other features that are not selected for FMD detection. Though their feature importance scores are not the highest, it is still possible that these features may contribute to the detection of some FN batteries. As is shown in Fig. 8, although the feature K1 and OCV3 of some TP batteries exceeds the distribution of normal batteries, all the 10 features of FN batteries are overlapped with the features of normal batteries respectively, which indicates that the 10 unselected features are not helpful for the FN detection. Therefore, taking the unselected features into account cannot improve the detection results. These results prove the reliability of the feature selection from another side. Finally, it is concluded that the FN batteries cannot be detected with the current collected features. Therefore, the maximum achievable Recall in this study is 62.07% (18/29).

The mechanism of the defect's impact on battery performance can be the ISC caused by the metal particles. The selected features K2 and OCV4 are relevant to self-discharge, hence they can indicate the ISC. There are two possible ways of forming ISC. Firstly, the separator on the side of the particle can be broken after hot-pressing. Then, with the volume

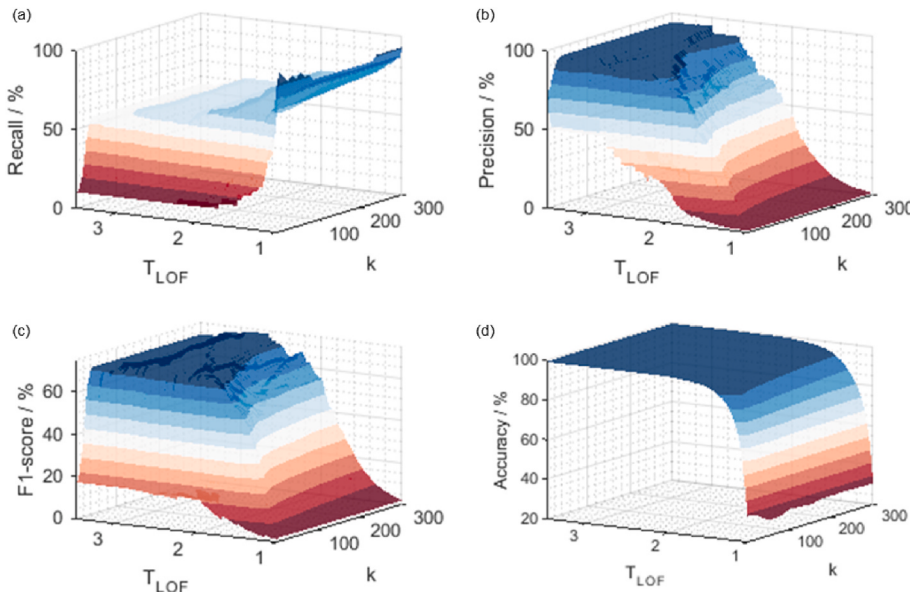


Fig. 6. The four indicators (a) Recall, (b) Precision, (c) F1-score, (d) Accuracy change with different hyperparameters.

Table 6
Results of the hyperparameter tuning.

Hyperparameter combinations	Recall	Precision	Accuracy
$k = 150, T_{\text{LOF}} \in [2.88, 2.89]$	62.07%	94.74%	99.70%
$k = 160, T_{\text{LOF}} \in [2.86, 2.90]$	62.07%	94.74%	99.70%
$k = 170, T_{\text{LOF}} \in [2.85, 2.92]$	62.07%	94.74%	99.70%
$k = 180, T_{\text{LOF}} \in [2.84, 2.90]$	62.07%	94.74%	99.70%
$k = 190, T_{\text{LOF}} \in [2.82, 2.90]$	62.07%	94.74%	99.70%
$k = 200, T_{\text{LOF}} \in [2.81, 2.91]$	62.07%	94.74%	99.70%
$k = 210, T_{\text{LOF}} \in [2.82, 2.89]$	62.07%	94.74%	99.70%
$k = 220, T_{\text{LOF}} \in [2.84, 2.90]$	62.07%	94.74%	99.70%
$k = 230, T_{\text{LOF}} \in [2.88, 2.92]$	62.07%	94.74%	99.70%
$k = 240, T_{\text{LOF}} \in [2.89, 2.93]$	62.07%	94.74%	99.70%
$k = 250, T_{\text{LOF}} \in [2.91, 2.93]$	62.07%	94.74%	99.70%
$k = 260, T_{\text{LOF}} \in [2.93, 2.94]$	62.07%	94.74%	99.70%

expansion of the battery during battery finishing process, the metal particle may contact with cathode and anode, causing the internal short circuit. Secondly, anodic corrosion of the metal particle can be triggered when the cathode potential is higher than the oxidation-reduction potential of the metal particle. The metal is dissolved and the ions transfer and deposit at anode during charging, which makes the metal grow through the separator and connect the anode and cathode and cause ISC. Although there are possibilities of ISC, the ISC still happens accidentally. If no ISC happens during battery finishing process, the self-discharge rate of the FMD battery won't be abnormal. Therefore, based on the mechanism analysis, the Recall value equals to 62.07% is reasonable. It is worth noting that, the Recall of the detection method is still 6 times higher than that of the HiPot methods.

4.6. Discussions on computational efficiency

The data-driven method has the potential to be deployed on the manufacturing execution system. For better application, the computational efficiency of the core algorithm is analyzed in the following.

Random Forest is an ensemble method, so its computational

efficiency (or computational complexities) is close to the sum of the complexities of individual DTs. Assuming the DTs all have the same complexity, then it would be the complexity of one DT times the number of DTs denoted by N_{DT} . The DTs used in the RF model are Classification and Regression Trees. Assuming we have N observations and M attributes, the computational cost of building a tree is $O(M^*N^*\log N)$. Then the complexity of the RF is $O(N_{\text{DT}}^*M^*N^*\log N)$. More information can be found in the book [54].

Local Outlier Factor can be regarded as a two-step algorithm. In the first step, the k nearest neighbors are found. The complexity of this step is $O(N^*\text{time for a } k\text{-NN query})$. For the k -NN queries, different methods can be used on different dimensional data. For high-dimensional data, a sequential scan or some variant of it need to be used, whose complexity is $O(N)$. Therefore, the complexity of the first step can be as large as $O(N^2)$. In the second step, the LOF values are calculated with the result of the first step instead of the original input. The time complexity of the second step is $O(N)$. Therefore, the complexity of the LOF algorithm can be as large as $O(N^2)$. More information can be found in Ref. [52].

In real application, the RF algorithm is only used once to select the important feature with the experiment data. After the feature selection, the LOF algorithm runs periodically (about once a day or twice a day) with the real manufacturing data. Using the computer with 8 GB memory and 4.97 GHz CPU, the time taken by the LOF algorithm using the experiment data as input is 0.09873s. Therefore, the computational efficiency is not a problem in real applications.

5. Conclusions

In this paper, we propose a data-driven detection method for foreign matter defect in lithium-ion batteries. In contrast to the existing battery diagnosis and fault detection methods that use battery operating data as input, we conducted the experiments and implanted foreign matter defects into batteries on a real battery pilot manufacturing line from which the data of FMD batteries and thousands of normal batteries were collected and used as input for defect detection. This research results are

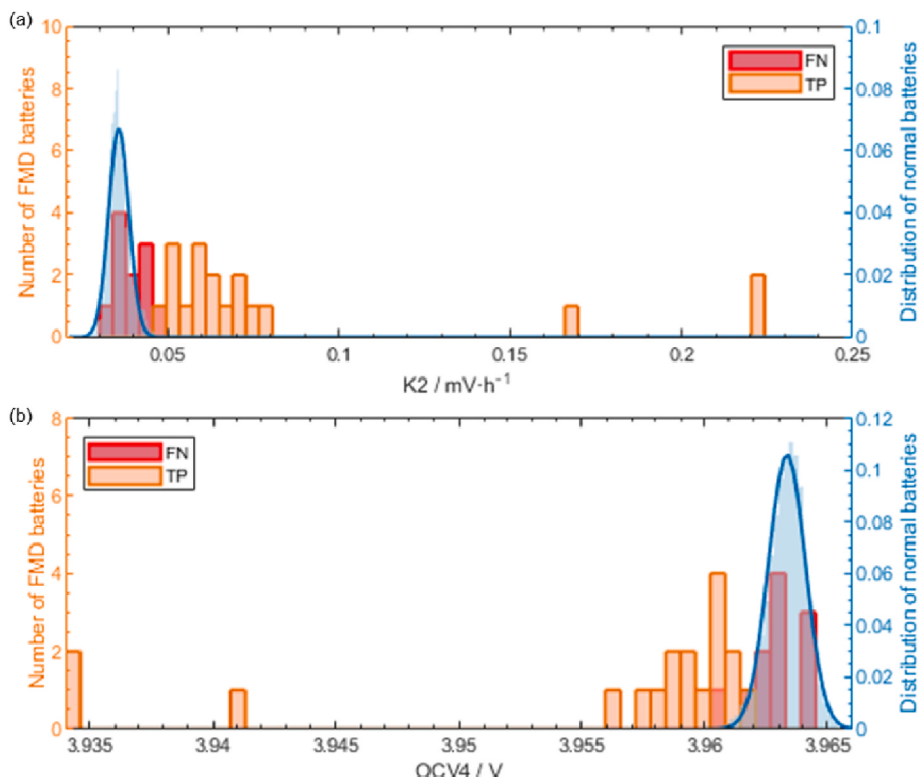


Fig. 7. (a) K_2 and (b) OCV_4 distribution of normal batteries and FMD batteries.

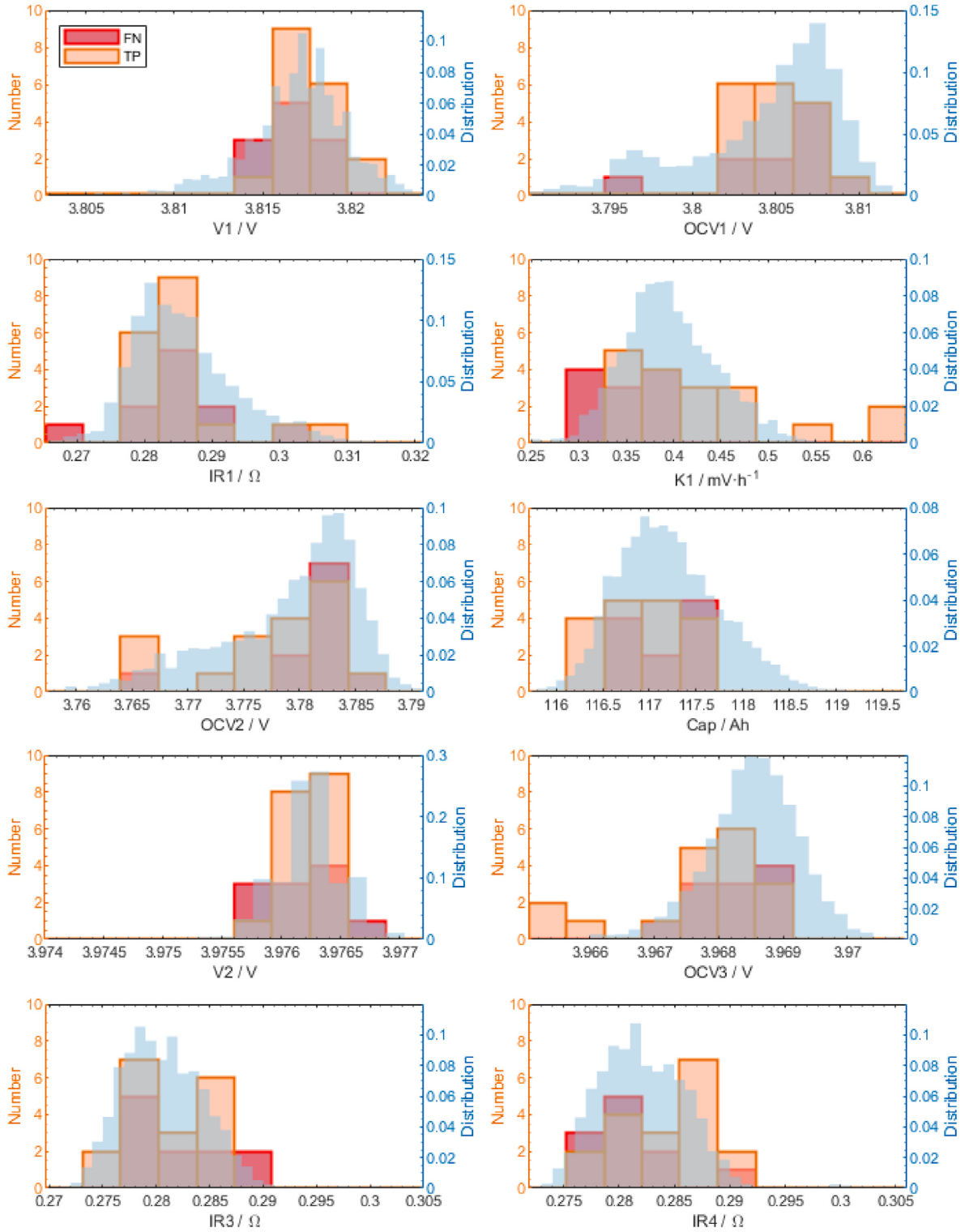


Fig. 8. Distribution of the unselected features of normal batteries and FMD batteries.

helpful to improve the battery safety from the manufacturing side.

Feature selection is conducted with feature importance analysis by using the RF method and OOB error calculation. Two features K2 and OCV4 which have the highest feature importance are selected from the 12 features and used as the input for FMD detection. The LOF algorithm is used for the FMD detection and achieves high Precision (94.74%), high Accuracy (99.70%) and the Recall (62.07%) is 6 times higher than the HiPot test used in the pilot manufacturing line. The method

introduced in this study has the potential to be deployed on the manufacturing execution system to further enhance the screening of defective batteries and improve the quality of battery production.

To make the method more practical, the algorithm will be validated with unlabeled batteries. Battery disassembly analyses will be carried out in our next-step research. The cycling performance of the FMD batteries will be analyzed and the abuse tests will be conducted. Further research on defective batteries will be conducted to improve battery

safety.

Credit author statement

Yue Pan: Data curation, Methodology, Software, Validation, Visualization, Writing - Original Draft, Xiangdong Kong: Data curation, Funding acquisition, Yuebo Yuan: Data curation, Validation, Yukun Sun: Data curation, Xuebing Han: Supervision, Funding acquisition, Hongxin Yang: Resources, Jianbiao Zhang: Resources, Xiaoan Liu: Resources, Panlong Gao: Resources, Yihui Li: Resources, Languang Lu: Supervision, Minggao Ouyang: Supervision, Project administration, Funding acquisition.

Declaration of competing interest

The authors declare that they have no known competing financial interests or personal relationships that could have appeared to influence the work reported in this paper.

Data availability

The data that has been used is confidential.

Acknowledgments

This work is supported by National Key R&D Program of China under the Grant No. 2019YFE0100200, National Natural Science Foundation of China under the Grant No. 52107226, No. 52177217 and No. 52037006, Beijing Natural Science Foundation under the Grant No. 3212031 and the China Postdoctoral Science Foundation under the Grant No. 2020TQ0167.

Appendix A. Supplementary data

Supplementary data to this article can be found online at <https://doi.org/10.1016/j.energy.2022.125502>.

References

- [1] Shahjalal M, Roy PK, Shams T, Fly A, Chowdhury JI, Ahmed MR, et al. A review on second-life of Li-ion batteries: prospects, challenges, and issues. Energy 2022;241:122881. <https://doi.org/10.1016/j.energy.2021.122881>.
- [2] Dixon J, Bell K. Electric vehicles: battery capacity, charger power, access to charging and the impacts on distribution networks. ETransportation 2020;4:100059. <https://doi.org/10.1016/j.etran.2020.100059>.
- [3] Zhang H, Zhang J. An overview of modification strategies to improve LiNi0.8Co0.1Mn0.1O2 (NCM811) cathode performance for automotive lithium-ion batteries. ETransportation 2021;7. <https://doi.org/10.1016/j.etran.2021.100105>.
- [4] Lai X, Huang Y, Gu H, Han X, Feng X, Dai H, et al. Remaining discharge energy estimation for lithium-ion batteries based on future load prediction considering temperature and ageing effects. Energy 2022;238:121754. <https://doi.org/10.1016/j.energy.2021.121754>.
- [5] McIlwaine N, Foley AM, Morrow DJ, Al Kez D, Zhang C, Lu X, et al. A state-of-the-art techno-economic review of distributed and embedded energy storage for energy systems. Energy 2021;229:120461. <https://doi.org/10.1016/j.energy.2021.120461>.
- [6] Olabi AG, Wilberforce T, Sayed ET, Abo-Khalil AG, Maghrabie HM, Elsaid K, et al. Battery energy storage systems and SWOT (strengths, weakness, opportunities, and threats) analysis of batteries in power transmission. Energy 2022;254:123987. <https://doi.org/10.1016/j.energy.2022.123987>.
- [7] Lin Q, Wang J, Xiong R, Shen W, He H. Towards a smarter battery management system: a critical review on optimal charging methods of lithium ion batteries. Energy 2019;183:220–34. <https://doi.org/10.1016/j.energy.2019.06.128>.
- [8] Hu G, Huang P, Bai Z, Wang Q, Qi K. Comprehensively analysis the failure evolution and safety evaluation of automotive lithium ion battery. ETransportation 2021;10:100140. <https://doi.org/10.1016/j.etran.2021.100140>.
- [9] Zhou Z, Zhou X, Cao B, Yang L, Liew KM. Investigating the relationship between heating temperature and thermal runaway of prismatic lithium-ion battery with LiFePO₄ as cathode. Energy 2022;256:124714. <https://doi.org/10.1016/j.energy.2022.124714>.
- [10] Mallarapu A, Kim J, Carney K, DuBois P, Santhanagopalan S. Modeling extreme deformations in lithium ion batteries. ETransportation 2020;4:100065. <https://doi.org/10.1016/j.etran.2020.100065>.
- [11] Yin H, Ma S, Li H, Wen G, Santhanagopalan S, Zhang C. Modeling strategy for progressive failure prediction in lithium-ion batteries under mechanical abuse. ETransportation 2021;7:100098. <https://doi.org/10.1016/j.etran.2020.100098>.
- [12] Li Y, Gao X, Feng X, Ren D, Li Y, Hou J, et al. Battery eruption triggered by plated lithium on anode during thermal runaway after fast charging. Energy 2022;239:122097. <https://doi.org/10.1016/j.energy.2021.122097>.
- [13] Huang P, Yao C, Mao B, Wang Q, Sun J, Bai Z. The critical characteristics and transition process of lithium-ion battery thermal runaway. Energy 2020;213:119082. <https://doi.org/10.1016/j.energy.2020.119082>.
- [14] Fan Z, Gao R, Liu S. Thermal conductivity enhancement and thermal saturation elimination designs of battery thermal management system for phase change materials based on triply periodic minimal surface. Energy 2022;259:125091. <https://doi.org/10.1016/j.energy.2022.125091>.
- [15] Guo C, Liu H, Guo Q, Shao X, Zhu M. Investigations on a novel cold plate achieved by topology optimization for lithium-ion batteries. Energy 2022;261:125097. <https://doi.org/10.1016/j.energy.2022.125097>.
- [16] Zhang X, Li Z, Luo L, Fan Y, Du Z. A review on thermal management of lithium-ion batteries for electric vehicles. Energy 2022;238:121652. <https://doi.org/10.1016/j.energy.2021.121652>.
- [17] Jilte R, Afzal A, Panchal S. A novel battery thermal management system using nano-enhanced phase change materials. Energy 2021;219:119564. <https://doi.org/10.1016/j.energy.2020.119564>.
- [18] Xu P, Hu X, Liu B, Ouyang T, Chen N. Hierarchical estimation model of state-of-charge and state-of-health for power batteries considering current rate. IEEE Trans Ind Inf 2022;18:6150–9. <https://doi.org/10.1109/TII.2021.3131725>.
- [19] Ouyang T, Xu P, Lu J, Hu X, Liu B, Chen N. Co-Estimation of state-of-charge and state-of-health for power batteries based on multi-thread dynamic optimization method. IEEE Trans Ind Electron 2021;69:1157–66. <https://doi.org/10.1109/TIE.2021.3062266>.
- [20] Qiao D, Wang X, Lai X, Zheng Y, Wei X, Dai H. Online quantitative diagnosis of internal short circuit for lithium-ion batteries using incremental capacity method. Energy 2022;243:123082. <https://doi.org/10.1016/j.energy.2021.123082>.
- [21] Jiang L, Deng Z, Tang X, Hu L, Lin X, Hu X. Data-driven fault diagnosis and thermal runaway warning for battery packs using real-world vehicle data. Energy 2021;234:121266. <https://doi.org/10.1016/j.energy.2021.121266>.
- [22] David L, Ruther RE, Mohanty D, Meyer HM, Sheng Y, Kalnaus S, et al. Identifying degradation mechanisms in lithium-ion batteries with coating defects at the cathode. Appl Energy 2018;231:446–55. <https://doi.org/10.1016/j.apenergy.2018.09.073>.
- [23] Qian G, Monaco F, Meng D, Lee SJ, Zan G, Li J, et al. The role of structural defects in commercial lithium-ion batteries. Cell Reports Phys Sci 2021;2:100554. <https://doi.org/10.1016/j.xcrp.2021.100554>.
- [24] WM Motor recall. https://www.samr.gov.cn/zw/zh/202010/t20201028_322686.html.
- [25] BMW PHEV recall. https://www.samr.gov.cn/zw/zh/202110/t20211019_335834.html.
- [26] Mohanty D, Hockaday E, Li J, Hensley DK, Daniel C, Wood DL. Effect of electrode manufacturing defects on electrochemical performance of lithium-ion batteries: cognizance of the battery failure sources. J Power Sources 2016;312:70–9. <https://doi.org/10.1016/j.jpowsour.2016.02.007>.
- [27] Fink KE, Polzin BJ, Vaughn JT, Major JJ, Dunlop AR, Trask SE, et al. Influence of metallic contaminants on the electrochemical and thermal behavior of Li-ion electrodes. J Power Sources 2022;518:230760. <https://doi.org/10.1016/j.jpowsour.2021.230760>.
- [28] Sa Q, Heelan JA, Lu Y, Apelian D, Wang Y. Copper impurity effects on LiNi1/3Mn1/3Co1/3O2 cathode material. ACS Appl Mater Interfaces 2015;7:20585–90. <https://doi.org/10.1021/acsami.5b04426>.
- [29] Yu W, Guo Y, Shang Z, Zhang Y, Xu S. A review on comprehensive recycling of spent power lithium-ion battery in China. ETransportation 2022;11:100155. <https://doi.org/10.1016/j.etran.2022.100155>.
- [30] Mostafaee M. Six Sigma for quality assurance of Lithium- ion batteries in the cell assembly process. 2021.
- [31] Zwicker MFR, Moghadam M, Zhang W, Nielsen CV. Automotive battery pack manufacturing - a review of battery to tab joining. J Adv Join Process 2020;1:100017. <https://doi.org/10.1016/j.jajp.2020.100017>.
- [32] Liu L, Feng X, Zhang M, Lu L, Han X, He X, et al. Comparative study on substitute triggering approaches for internal short circuit in lithium-ion batteries. Appl Energy 2020;259:114143. <https://doi.org/10.1016/j.apenergy.2019.114143>.
- [33] Thermal Propagation Topics. Effect of induced metal contaminants on lithium-ion cell safety. EVS1536-613, <https://wiki.unece.org/display/trans/EVS+15th+session>.
- [34] Kong X, Lu L, Yuan Y, Sun Y, Feng X, Yang H, et al. Foreign matter defect battery and sudden spontaneous combustion. ETransportation 2022;12:100170. <https://doi.org/10.1016/j.etran.2022.100170>.
- [35] Sun Y, Yuan Y, Lu L, Han X, Kong X, Wang H, et al. A comprehensive research on internal short circuits caused by copper particle contaminants on cathode in lithium-ion batteries. ETransportation 2022;13:100183. <https://doi.org/10.1016/j.etran.2022.100183>.
- [36] Etiemble A, Besnard N, Adrien J, Tran-Van P, Gautier L, Lestriez B, et al. Quality control tool of electrode coating for lithium-ion batteries based on X-ray radiography. J Power Sources 2015;298:285–91. <https://doi.org/10.1016/j.jpowsour.2015.08.030>.
- [37] Gitis A. Flaw detection in the coating process of lithium-ion battery electrodes with acoustic guided waves 2017.

- [38] Sharp N, Oregan P, Adams D, Caruthers J, David A, Suchomel M. Lithium-ion battery electrode inspection using pulse thermography. *NDT E Int* 2014;64:41–51. <https://doi.org/10.1016/j.ndteint.2014.02.006>.
- [39] Badmos O, Kopp A, Bernthaler T, Schneider G. Image-based defect detection in lithium-ion battery electrode using convolutional neural networks. *J Intell Manuf* 2020;31:885–97. <https://doi.org/10.1007/s10845-019-01484-x>.
- [40] Xu C, Li L, Li J, Wen C. Surface defects detection and identification of lithium battery Pole piece based on multi-feature fusion and PSO-SVM. *IEEE Access* 2021;9:85232–9. <https://doi.org/10.1109/ACCESS.2021.3067641>.
- [41] Wu Y, Saxena S, Xing Y, Wang Y, Li C, Yung WKC, et al. Analysis of manufacturing-induced defects and structural deformations in lithium-ion batteries using computed tomography. *Energies* 2018;11. <https://doi.org/10.3390/en11040925>.
- [42] Peng J, Xue M, Lou Y. Automatic internal wrinkles detection of lithium-ion batteries using convolutional neural network. *IEEE Int Conf Autom Sci Eng* 2021;8:23–7. <https://doi.org/10.1109/CASE49439.2021.9551649>. 2021.
- [43] Bauermann LP, Mesquita LV, Bischoff C, Drews M, Fitz O, Heuer A, et al. Scanning acoustic microscopy as a non-destructive imaging tool to localize defects inside battery cells. *J Power Sources Adv* 2020;6:100035. <https://doi.org/10.1016/j.powera.2020.100035>.
- [44] Robinson JB, Engebretsen E, Finegan DP, Darr J, Hinds G, Shearing PR, et al. Detection of internal defects in lithium-ion batteries using lock-in thermography. *ECS Electrochem Lett* 2015;4:A106–9. <https://doi.org/10.1149/2.0071509eel>.
- [45] Ma L, Xie W, Zhang Y. Blister defect detection based on convolutional neural network for polymer lithium-ion battery. *Appl Sci* 2019;9. <https://doi.org/10.3390/app9061085>.
- [46] Leithoff R, Fröhlich A, Masuch S, Ventura Silva G, Dröder K. Process-product interdependencies in lamination of electrodes and separators for lithium-ion batteries. *Energy* 2022;15:1–17. <https://doi.org/10.3390/en15072670>.
- [47] Hoffmann L, Kasper M, Kahn M, Gramse G, Silva GV, Herrmann C, et al. High-potential test for quality control of separator defects in battery cell production. *Batteries* 2021;7. <https://doi.org/10.3390/batteries7040064>.
- [48] Shan H, Cao H, Xu X, Xiao T, Hou G, Cao H, et al. Investigation of self-discharge properties and a new concept of open-circuit voltage drop rate in lithium-ion batteries. *J Solid State Electrochem* 2022;26:163–70. <https://doi.org/10.1007/s10008-021-05049-y>.
- [49] Janitzka S, Strobl C, Boulesteix AL. An AUC-based permutation variable importance measure for random forests. *BMC Bioinf* 2013;14. <https://doi.org/10.1186/1471-2105-14-119>.
- [50] Breiman L. Random forests. *Mach Learn* 2001;45:5–32. <https://doi.org/10.1023/A:1010933404324>.
- [51] Liu K, Hu X, Zhou H, Tong L, Widanage WD, Marco J. Feature analyses and modeling of lithium-ion battery manufacturing based on random forest classification. *IEEE/ASME Trans Mechatronics* 2021;26:2944–55. <https://doi.org/10.1109/TMECH.2020.3049046>.
- [52] Breunig MM, Kriegel H-P, Ng RT, Sander JLOF. Identifying density-based local outliers. In: Proc. 2000 ACM SIGMOD Int. Conf. Manag. Data. New York, USA: ACM Press; 2000. p. 93–104. <https://doi.org/10.1145/342009.335388>.
- [53] Zhao Y, Liu P, Wang Z, Zhang L, Hong J. Fault and defect diagnosis of battery for electric vehicles based on big data analysis methods. *Appl Energy* 2017;207:354–62. <https://doi.org/10.1016/j.apenergy.2017.05.139>.
- [54] Witten IH, Frank E, Hall MA, Pal CJ, Data M. Practical machine learning tools and techniques. In: Data mining, vol. 2; 2005. No. 4.